Coupled-surface investigation of the photodissociation of NH$_3(\widetilde{A})$: Effect of exciting the symmetric and antisymmetric stretching modes

David Bonhommeau,[1] Rosendo Valero,[1] Donald G. Truhlar,[1,a)] and Ahren W. Jasper[2]

[1]*Department of Chemistry and Supercomputing Institute, University of Minnesota, 207 Pleasant Street SE, Minneapolis, Minnesota 55455-0431, USA*
[2]*Combustion Research Facility, Sandia National Laboratories, P.O. Box 969, Livermore, California 94551-0969, USA*

Using previously developed potential energy surfaces and their couplings, non-Born–Oppenheimer trajectory methods are used to study the state-selected photodissociation of ammonia, prepared with up to six quanta of vibrational excitation in the symmetric (ν_1) or antisymmetric (ν_3) stretching modes of NH$_3(\widetilde{A})$. The predicted dynamics is mainly electronically nonadiabatic (that is, it produces ground electronic state amino radicals). The small probability of forming the excited-state amino radical is found, for low excitations, to increase with total energy and to be independent of whether the symmetric or antisymmetric stretch is excited; however some selectivity with respect to exciting the antisymmetric stretch is found when more than one quantum of excitation is added to the stretches, and more than 50% of the amino radical are found to be electronically excited when six quanta are placed in the antisymmetric stretch. These results are in contrast to the mechanism inferred in recent experimental work, where excitation of the antisymmetric stretch by a single quantum was found to produce significant amounts of excited-state products via adiabatic dissociation at total energies of about 7.0 eV. Both theory and experiment predict a broad range of translational energies for the departing H atoms when the symmetric stretch is excited, but the present simulations do not reproduce the experimental translational energy profiles when the antisymmetric stretch is excited. The sensitivity of the predicted results to several aspects of the calculation is considered in detail, and the analysis leads to insight into the nature of the dynamics that is responsible for mode selectivity. © *2009 American Institute of Physics.*
[DOI: 10.1063/1.3132222]

I. INTRODUCTION

The photodissociation of ammonia to produce amino radical and a hydrogen atom has been studied by various experimental methods,[1–14] culminating in two sets of very detailed experiments (by Doppler profile spectroscopy[11,13] and by velocity map imaging[14]) in the Crim laboratory. These experiments[11,13,14] give detailed information about the product translational energy distribution when the symmetric stretch (ν_1), umbrella mode (ν_2), and antisymmetric stretch (ν_3) of the $\widetilde{A}$ first-excited-singlet electronic state (S_1) of ammonia (which has a planar geometry) is initially excited, complementing earlier experiments from the Dixon laboratory[2] on the role of excitation of ν_2. The product translational energy distribution has been interpreted in terms of the propensity to produce electronically excited amino radicals as a function of the initial vibrational state, and hence these experiments provide insight into the mechanism of state-selected photochemistry.

Bach *et al.*[11,13] and Hause *et al.*[14] found that the fragmentation of NH$_3(\widetilde{A})$ molecules excited in one of their antisymmetric stretching modes mainly produced slow H atoms, whereas NH$_3(\widetilde{A})$ molecules excited in their symmetric stretching mode produced a faster distribution of H atoms. They have interpreted the surprising production of slow H atoms as a signature of an electronically adiabatic dissociation process producing electronically excited amino radical. They concluded that dissociation is preferentially adiabatic when the antisymmetric stretching mode is excited and nonadiabatic when the symmetric stretching mode is excited.

Although systems with only a few atoms, such as ammonia, are amenable to quantum mechanical simulations based on scattering theory[15] or wave packets,[16] there is considerable interest in less computationally demanding approaches that can be applied to large systems without dimensionality-reduction approximations. The quasiclassical (QC) trajectory method[17,18] provides such an approach for Born–Oppenheimer (i.e., electronically adiabatic) processes, and coupled-surface trajectory methods[19,20] provide such an approach for non-Born–Oppenheimer processes. A second advantage of trajectory-based approaches is that, if successful, they provide opportunities for mechanistic interpretation in terms of phase space paths and classical concepts.

We have developed coupled-surface trajectory methods of two types,[20–28] namely, Ehrenfest-like[29,30] methods and trajectory surface hopping[31–34] methods. The most accurate, in general, is coherent switching with decay of mixing[21–24] (CSDM), which is an Ehrenfest-like method, but another ap-

---

a)Electronic mail: truhlar@umn.edu.

proach that provides useful accuracy in many cases is fewest switches with time uncertainty[25–27] (FSTU), which is a trajectory surface-hopping method. The FSTU method has recently been further refined, yielding FSTU with stochastic decoherence (FSTU/SD).[28]

These methods have previously been used to study the photodissociation of $NH_3(\widetilde{A})$ as a function of n_2 (the number of quanta of vibrational excitation in ν_2).[35] The objective of the present study is the photodissociation of $NH_3(\widetilde{A})$ as a function of vibrational excitation of the symmetric and antisymmetric stretches.

Two previous theoretical studies of the photodissociation dynamics of ammonia are noteworthy here. Seideman[36] has published a detailed, reduced dimensionalilty, quantum mechanical study of the predissociation of the ammonia $\widetilde{A}$ state in the ground vibrational state, and several rotational-vibrational states involving bend excitation. In the energy range of interest to her, photofragments form exclusively in ground electronic state.[2] More recently, Lai *et al.*[37] reported a full-dimensional wave packet study of the NH_3 photodissociation dynamics by using the same potential energy surfaces (PESs) as in the present study. Although the latter study did not report any product branching that might be compared to experiment or with the present study, Lai *et al.* did find that their calculations correctly reproduced some experimental observables such as the dependence of lifetime on excitation energy for low-lying resonances in which the umbrella mode is excited and the overall shape of the spectra when stretching modes are excited. They concluded that their results "confirmed the general accuracy of the newly developed PESs of Truhlar and coworkers."

Since the state preparation in the experiments of Crim and co-workers[11,13,14] is by a novel double resonance technique,[38] it is important to keep in mind the initial state preparation used in the present study and how it relates to the experimental initial conditions. The experiments involve two-photon state preparation, beginning in the ground electronic state. The first photon prepares a specific vibrationally excited state of the ground electronic state, and the second photon excites the system to the excited $\widetilde{A}$ electronic state. Although the second photon does not place the system in a single well resolved eigenstate [such eigenstates do not exist for ammonia at the energies of most interest in the present study because the spectrum is diffuse at energies above 5.7 eV (Ref. 39)], the Franck–Condon principle implies that electronic excitation of a vibrationally excited state will preferentially produce excited states composed of zero-order states that have the same character of vibrational motion as the intermediate state produced after one photon is absorbed.[38] Thus a difference in outcomes between exciting the symmetric and antisymmetric vibrations before electronic excitation was interpreted[11,13,14] as resulting from "preparation of otherwise inaccessible vibrations in the electronically excited molecules by bringing different Franck–Condon factors into play."[14,38,40] A semiclassical trajectory calculation cannot completely mimic the quantum state preparation of a real experiment, but we have adopted state preparation schemes that we believe allow us to test the con-

clusions drawn from the experiments, or alternatively to test the ability of our semiclassical methods and PESs to yield the state specificity observed experimentally. In particular, our initial state for the symmetric-stretch-mediated case is a QC analog of a zero-order approximation to a vibrationally excited state with that same vibrational character on the excited PES. The zero-order state is bound because it is based on the harmonic approximation using the upper surface, but when the trajectory begins to evolve, it is propagated using the accurate PESs, and thus it can dissociate. Similarly, our initial trajectory state for the antisymmetric-stretch-mediated case is a QC or analog of a zero-order approximation to a vibrationally excited state with antisymmetric-stretch character on the upper PES. In principle these states might be more pure than the actual states excited in the experiment, and could, under that same principle, lead to more state-specific behavior than is observed experimentally, but this hypothetical possibility is not a major concern.

The methodology adopted in this work is presented in Sec. II. Results obtained with four different coupled-surface trajectory methods are presented and discussed in Sec. III. Section IV gives concluding remarks.

II. METHODS

Section II.A provides an overview of the essential features of the methodology, including all features that differ from or extend our previous publication.[35] The algorithm for simulation of initial vibrational distributions of photoexcited molecules is presented in Sec. II.B. Section II.C discusses the main features of the PESs employed and the vibrational states studied in the present work, and Sec. II.D details the method used to study intermode couplings.

II.A. Dynamics

In trajectory surface-hopping calculations, the classical motion of the nuclei is governed at any one time by a single PES, and this single-surface propagation is interrupted by transitions between surfaces, also called hops or switches. For a two-state case, the normalized electronic wave function is written as

$$\Phi = c_1(t)\phi_1(\mathbf{R}(t)) + c_2(t)\phi_2(\mathbf{R}(t)), \quad (1)$$

where t is time, $\mathbf{R}$ denotes the collection of nuclear coordinates, and ϕ_j is the normalized electronic wave function corresponding to surface j (note that the $\{\phi_j\}$ are orthogonal). The local rate of change of c_j along the classical trajectory is computed using well-known semiclassical equations,[19] and hops are allowed stochastically according to the fewest-switches prescription[34] such that if all attempted hops occurred, the probability of propagating on each surface j would be equal to $|c_j|^2$. For an ensemble of trajectories, this self-consistency implies that the fraction of trajectories propagating in each state is equal to the ensemble-averaged quantum mechanical populations $\langle|c_j|^2\rangle$, although this self-consistency is not always maintained (as discussed in the next paragraph). When a hop occurs, the nuclear momentum is adjusted in the direction of the nonadiabatic coupling direction $\hat{\mathbf{d}}$ such that the total energy is conserved.

Frequently in multidimensional systems, a hopping attempt to an excited electronic state may be requested by the fewest-switches algorithm at a geometry where the potential energy gap is greater than the kinetic energy associated with nonadiabatic coupling direction $\hat{\mathbf{d}}$. When this is the case, the kinetic energy along $\hat{\mathbf{d}}$ cannot be adjusted such that total energy is conserved, and these events are called frustrated hops. In some implementations of the fewest-switches algorithm, frustrated hops are ignored, and this is one reason that the self-consistency discussed above is not preserved. The FSTU method is a modification of the fewest-switches method designed to improve self-consistency; the FSTU method differs from the fewest-switches method in that it allows[25,26] hops to occur at some time t_h along the classical trajectory if a hop is frustrated at t_0 but allowed at t_h and if

$$|t_0 - t_h| \le \frac{\hbar}{2\Delta E}, \tag{2}$$

where $\hbar$ is Planck's constant (h) divided by 2π, and ΔE is the energy that would need to be borrowed at t_0 to allow a hop. A second improvement is the use of the gradV criterion[27] for determining whether a momentum adjustment is made for frustrated trajectories.

We also consider the stochastic decoherence[28] (SD) modification to the FSTU method. In the SD method, decoherence events occur stochastically according to characteristic decoherence time τ defined as the time for phenomenological decay of the off-diagonal elements of the electronic density matrix due to imagined nuclear wave packets propagating in the different electronic states at different velocities.[41] When a decoherence event is called for, the electronic coefficients c_j are reinitialized to the currently occupied electronic state. The prescription for SD was given incorrectly in Ref. 28; the correct probability of electronic reinitialization is given by

$$P(\Delta t) = \exp(-\Delta t / \tau), \tag{3}$$

where Δt is the time since the previous reinitialization check. Reinitialization checks are made at every time step in the current work.

In quantum mechanical dynamics, vibrational energy is strictly quantized only in stationary states, and therefore zero-point energy (ZPE) is not strictly maintained during collisions or in metastable dissociative states. However, experience has shown that maintaining ZPE in motions with positive local force constants leads to more accurate reaction thresholds,[42] and maintaining ZPE throughout a trajectory is the most convenient way to ensure that all product states have their required ZPE. Algorithmically though, maintaining ZPE in classical trajectory simulations has been an unmet challenge for decades.[17,35,43–53] Due to severe shortcomings of earlier ZPE maintenance methods,[44,45,48] a new scheme, called trajectory projection onto ZPE orbit (TRAPZ), was proposed by Lim and McCormack[47] and McCormack *et al.*[49,51] It was assumed to remove spurious features from the dynamics, but it was recently found[35] that it leads to unphysical results when used to model the photodissociation dynamics of NH$_3$($\tilde{A}$). Furthermore, we obtained unphysical

results when we did not maintain ZPE. The TRAPZ algorithm was then modified[35] to give birth to the minimal TRAPZ (mTRAPZ) method. This new algorithm, combined with the FSTU/SD surface-hopping technique, was successfully applied to photodissociation of NH$_3$($\tilde{A}$) to maintain ZPE.

The application conditions of the mTRAPZ method are slightly changed here as compared to our earlier publication. We have previously noticed[35] that performing an instantaneous normal mode analysis in Cartesian coordinates may result in inaccuracies when estimating the instantaneous projected Hessian. This difficulty was overcome by not applying the mTRAPZ algorithm when a geometry corresponding to an inaccurate instantaneous projected Hessian was identified. However, identifying these inaccuracies is difficult in practice because of the six degrees of freedom of ammonia. In the present study, the mTRAPZ algorithm is thus only applied when there are at most six nonzero frequencies, a frequency (either real or imaginary) being assumed to be zero when its modulus is below 1 cm^{-1}. This criterion was found (i) to shield trajectories from artifacts like the nonconservation of total angular momentum (a discrepancy that occurred for about 1%–2% of trajectories in our previous study[35]), and (ii) to maintain ZPE.

We also briefly report some results obtained using the CSDM method,[21,22,24] which is a modified mean-field method that incorporates phenomenological demixing to produce quantized final electronic states. Although the CSDM method is believed to be more accurate than FSTU or FSTU/SD in general,[21,22,24] we used the FSTU and FSTU/SD methods for most of the calculations presented here because these algorithms are easier than CSDM to combine with mTRAPZ and because these algorithms allow us to analyze the trajectories more easily, which is important in the present exploratory study.

The FSTU, FSTU/SD, FSTU+mTRAPZ, FSTU/SD +mTRAPZ, and CSDM methods are part of the ANT 08 (Ref. 54) package. The photodissociation results reported in this paper correspond to averages over 3000 or 5000 trajectories, except when otherwise noted. The analytic PESs and couplings used here were described previously.[55] Trajectories are propagated in the adiabatic representation, and whenever we refer to the PESs in the rest of this article, we are referring to the electronically adiabatic ones. A trajectory is considered dissociated when either one of the three N–H bond distances is at least 10.0 Å during 50 consecutive time steps, or when the total time exceeds 100 ps.

II.B. Trajectory harmonic initial conditions

Initial conditions are similar to those employed in our previous work.[35] In all the photodissociation calculations reported here, the initial conditions for the vibrational modes are determined in the harmonic approximation.

Vibrational modes that are initially in their ground state (vibrational quantum number n_m of mode m is zero) are in some cases initialized by using a Wigner distribution[56] and in some cases are initialized quasiclassically. We used both methods for two reasons: (1) We wanted to check whether

our main conclusions depend on this choice (we will see that they do not). (2) We believe that the Wigner distribution is more reasonable for modes in their ground vibrational state whereas the QC method is more appropriate for modes that are excited. Normal modes that are excited ($n_m > 0$) are always initialized quasiclassically. In Sec. III we will indicate which calculations use the QC prescription for ground-state modes and which ones use the Wigner prescription for ground-state modes. For completeness this subsection summarizes the harmonic QC method for initializing a vibrational mode m.

Note that when we label the vibrational modes $m = 1, 2, \ldots, 3N-6$, we order the frequencies ω_m in order of decreasing real value (if there is an imaginary frequency, it is ordered last, i.e., as mode M where $M = 3N-6 = 6$). This convention is used for discussing vibrational coordinates and momenta. However, at the equilibrium geometry of ammonia in either the ground or excited electronic state, two modes are degenerate. When we need to take account of this, especially to compare to experiment, we label the modes $k = 1, 2, 3, 4$; and we label the frequencies ν_k and order them in the usual way by symmetry. Thus, at the equilibrium geometries, $\omega_1 = \omega_2 = \nu_3$, $\omega_3 = \nu_1$, $\omega_4 = \omega_5 = \nu_4$, and $\omega_6 = \nu_2$.

It is convenient to use isoinertial mass-scaled Cartesian coordinates defined by

$$\tilde{q}_{\alpha\gamma} = \sqrt{\frac{m_\alpha}{\mu}} q_{\alpha\gamma}, \tag{4}$$

where m_α is the mass of atom α, μ is a constant mass (taken as 1 amu but no results depend on this choice), $\alpha = 1, 2, \ldots, N$, and $\gamma = x$, y, or z. The conjugate momenta $\tilde{p}_{\alpha\gamma}$ have a reduced mass of μ. All frequencies are given in wave numbers. We will consider two kinds of trajectories, those initiated at the photoexcited reactant and those initiated at the transition state on the electronically excited surface.

The initial conditions for reactant-initiated trajectories in this study correspond to definite vibrational quantum numbers in the planar excited $\tilde{A}$ state and are based on a normal mode analysis for that equilibrium structure. The normal mode analysis is performed at the equilibrium geometry to determine the frequencies ω_m and normal mode eigenvectors $\mathbf{L}_m$. Then the vibrational energy to be assigned to a given mode is calculated harmonically as

$$\varepsilon_{\text{vib},m} = \left(n_m + \tfrac{1}{2}\right) hc\omega_m, \tag{5}$$

where c is the speed of light. The mass-scaled harmonic classical turning point is calculated as

$$t_m = \frac{1}{2\pi c\omega_m} \sqrt{\frac{2\varepsilon_{\text{vib},m}}{\mu}} \tag{6}$$

and the initial mass-scaled coordinates are calculated as

$$\tilde{q}_{\alpha\gamma} = \tilde{q}_{e,\alpha\gamma} + \Delta\tilde{q}_{m,\alpha\gamma} = \tilde{q}_{e,\alpha\gamma} + \sum_{m=1}^{3N-6} L_{m,\alpha\gamma}\Delta_m, \tag{7}$$

where $L_{m,\alpha\gamma}$ is the component of the normal vector of mode m corresponding to the γ coordinate of atom α,

$$\Delta_m = t_m \cos(2\pi\xi_m), \tag{8}$$

and ξ_m is a quasirandom number in the interval (0,1]. Next the harmonic kinetic energy in mode m is calculated by

$$T_m = \varepsilon_{\text{vib},m} - \tfrac{1}{2}\mu(2\pi c\omega_m)^2(\Delta_m)^2 \tag{9}$$

and the components of the conjugate momenta are

$$\tilde{p}_{m,\alpha\gamma} = \pm \sum_{m=1}^{3N-6} L_{m,\alpha\gamma}\sqrt{2\mu T_m}, \tag{10}$$

where the sign is determined by another quasirandom number.

For the doubly degenerate antisymmetric stretch, an excitation of one or more quanta of vibration is modeled by half of the quanta in each degenerate mode. We have however checked that exciting the molecule with all the quanta of vibration in one degenerate mode and only ZPE in the other does not change the results in any significant way over a batch of trajectories.

The initial coordinates and momenta for the trajectories are obtained by unscaling the coordinates and momenta obtained in Eqs. (7) and (10), respectively, to obtain two new sets, $q_{\alpha\gamma}$ and $p_{\alpha\gamma}$. The set of $q_{\alpha\gamma}$ coordinates is then used to calculate the actual potential energy in the $\tilde{A}$ state, $V(q_{\alpha\gamma})$, which is added to the sum of the kinetic energies of the $3N-6$ modes calculated by Eq. (9) and to the potential energy, V_{min}, of the planar minimum of the $\tilde{A}$ state to obtain the total energy relative to the equilibrium geometry of the ground electronic state ammonia,

$$E_{\text{tot}} = \sum_{m=1}^{3N-6} T_m + V(q_{\alpha\gamma}) + V_{\text{min}}. \tag{11}$$

In some calculations, the coordinates and momenta obtained by the method just described are employed without further considerations as the initial conditions for the trajectory, which leads to a rather broad distribution of total energies due to the anharmonicity of the potential. This scheme is labeled energetically unrestrained (EU). In a second scheme, the total energy obtained in Eq. (11) is compared with the requested total energy for the trajectory, given by

$$\begin{aligned} E_{\text{tot}}(\text{harmonic}) &= \sum_{m=1}^{3N-6} \varepsilon_{\text{vib},m} + V_{\text{min}} \\ &= \sum_{k=1}^{4} (n_k + d_k/2)hc\nu_k + V_{\text{min}}, \end{aligned} \tag{12}$$

where n_k is the number of quanta in mode k, d_k is the degeneracy of mode k ($d_1 = d_2 = 1$, $d_3 = d_4 = 2$), and ν_k is the harmonic frequency (in cm^{-1}) in the $\tilde{A}$ state. If the total energy calculated in Eq. (11) differs from that in Eq. (12) by more than $\Delta E = 0.1$ eV, this set of initial conditions is discarded, and a new set of quasirandom initial conditions is generated; the process is repeated until the $\Delta E \leq 0.1$ eV condition is fulfilled. This scheme is labeled the $\Delta E = 0.1$ eV scheme. The two schemes have different advantages and disadvantages. Scheme 1 generates a more complete sampling of initial vibrational phases but a larger distribution of energies;
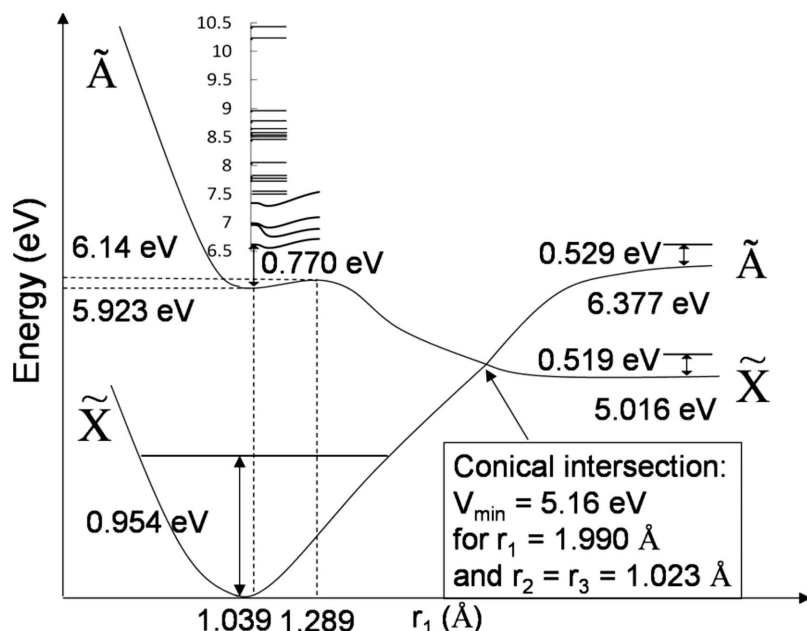
FIG. 1. Energy as a function of the longest N–H bond distance for the two lowest adiabatic states of NH₃ based on fitted adiabatic surfaces from Ref. 55. The three N–H distances are denoted as r_i ($i \in \{1,2,3\}$). The minimum of the $\tilde{A}$ electronic state is planar with $r_1 = r_2 = r_3 = 1.039$ Å (D_{3h} symmetry). The saddle point is planar with $r_1 = 1.289$ Å and $r_2 = r_3 = 1.040$ Å (C_{2v} symmetry), and the lowest-energy conical intersection is also planar. The minimum of the $\tilde{X}$ state is tetrahedral with $r_1 = r_2 = r_3 = 1.016$ Å. The zero of energy is the minimum of the ground electronic state. Reactant (i.e., NH₃) as well as product (i.e., NH₂) ZPEs are indicated. The vibrationally adiabatic curves for four sets of vibrational quantum numbers (see Fig. 2 for labeled curves) are represented above the segment of the reaction path comprised between the minimum of the $\tilde{A}$ electronic state and its saddle point. The energies of all the remaining vibrational levels studied in the present work are also indicated. Note that the diagram is only schematic (not to scale) between 1 and 5 eV and beyond 2 Å to make relevant quantities more discernible.

scheme 2 generates a narrow (0.2 eV) distribution of energies, but at the cost of limiting the phase average. To ascertain whether the results are sensitive to the way that initial conditions are generated we employed both schemes.

For the potential surface used here, $\nu_1 = 2777$ cm⁻¹ (symmetric stretch), $\nu_2 = 978$ cm⁻¹ (out-of-plane bend, i.e., umbrella mode), $\nu_3 = 3041$ cm⁻¹ (antisymmetric stretch), and $\nu_4 = 1330$ cm⁻¹ (in-plane bend). The umbrella frequency is scaled to a value of 892 cm⁻¹ in some of the calculations to better match the total energies used in the experiments. Note that all calculations in our previous study[35] used the scaled frequency. In the following we will always indicate whether we used the frequency of the umbrella mode predicted by the potential surface ($\nu_2 = 978$ cm⁻¹) or we used the scaled frequency (892 cm⁻¹).

We also consider trajectories initiated at the transition state, which is a hypersurface passing through the saddle point for electronically adiabatic dissociation in the $\tilde{A}$ state. The $3N-7$ bound modes of the transition state with the frequencies 3078, 3057, 1418, 1108, and 570 cm⁻¹ are sampled quasiclassically as discussed above, and the total energy is obtained as in Eq. (11). The energy along the reaction coordinate is then taken as

$$E_{\mathrm{rc}} = E_{\mathrm{vib}}(\text{harmonic, reactant}) - E_{\mathrm{vib}}(\text{harmonic, saddle}) - E_b,$$
(13)

where E_{vib} is the sum of the vibrational energies of all the bound modes ($3N-6$ modes for the first term and $3N-7$ modes for the second term), and E_b is the forward barrier height (0.22 eV). If E_{rc} is greater than zero, this energy is added along the reaction coordinate (with the momentum in the direction of the bimolecular products), otherwise no energy is added along the reaction coordinate. This procedure, involving the initiation of trajectories at the quantized transition state, may be considered to be a surface-hopping analog of the single-surface unified dynamical model[57–59] presented previously. The unscaled reactant umbrella frequency

of 978 cm⁻¹ was employed in these calculations, and the EU scheme was employed.

II.C. Potential energy surfaces and vibrational states

All dynamics calculations in the present article are carried out in the electronically adiabatic representation in which the adiabatic surfaces are coupled in the usual way[60] by the scalar product of the nonadiabatic coupling vector **d** and the velocity vector. The potential energy surfaces and couplings used here are the same as those used previously in the semiclassical dynamics study of Ref. 35. In particular, the PESs used in the present study for the ground ($\tilde{X}$) and the first excited ($\tilde{A}$) electronic state are computed from an analytical fit to the diabatic potentials and scalar coupling that are described in Ref. 55. (An earlier version of the surfaces and couplings has also been published.[61]) The adiabatic surfaces are computed by diagonalizing the diabatic potential energy matrix, and the nonadiabatic coupling vector **d** is computed analytically from the eigenvectors by a procedure explained elsewhere.[62]

A schematic that includes the location of the stationary points and the reaction paths on the adiabatic electronic states and the lowest-energy conical intersection is shown in Fig. 1. The ZPEs of the global minima of the $\tilde{X}$ and $\tilde{A}$ potential surfaces and of the NH₂ product in its ground and first excited state are also indicated.

Vibrationally adiabatic curves were calculated for some of the vibrational states used in the present study and they are also depicted in Fig. 1. The POLYRATE (Ref. 63) program package was used for this purpose. In these calculations, a minimum energy path (MEP) in isoinertial coordinates was constructed starting at the transition state and proceeding down to the reactant, i.e., to the minimum of the $\tilde{A}$ potential. The progress variable along this path is denoted s with $s = 0$ at the saddle point, and s negative at the reactant. Then, $3N-7$ generalized normal mode vibrational frequencies were calculated from the projected Hessian[58] (i.e., removing the
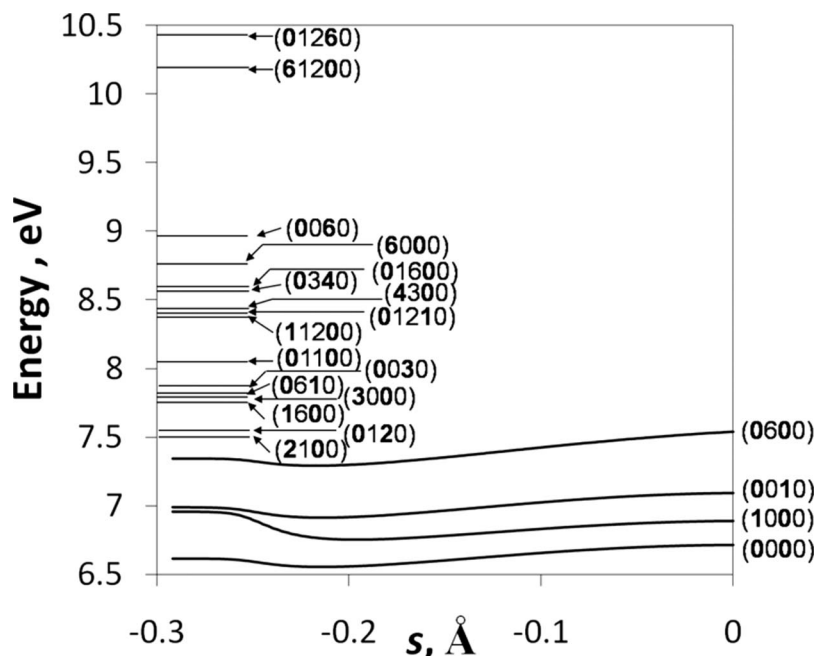
FIG. 2. Blowup of a key portion of Fig. 1 showing vibrationally adiabatic potential curves for the (0000), (1000), (0010), and (0600) states and energy levels for the remaining states studied in the present work. Vibrational quanta for ν_1 and ν_3 are indicated in bold to avoid confusion. The zero of energy is the minimum of the ground electronic state.

reaction coordinate mode) at intervals of 0.0025 Å along the reaction path. The frequencies were calculated in curvilinear coordinates. Four examples of the vibrationally adiabatic potential curves[58] are shown in Figs. 1 and 2. (Figure 2 is a blow-up of the most significant region of configuration space of Fig. 1.) The vibrationally adiabatic curves shown indicate that if the system evolves vibrationally adiabatically from the minimum geometry, vibrationally adiabatic barriers will be encountered in all the vibrational states except the (1 0 0 0) state. The energies of other initial vibrational states studied here are also indicated in these two figures, and Fig. 2 indicates the quanta of excitation in each mode for all the states.

II.D. Mode populations

If a quantum mechanical system in an uncoupled electronic state were initialized in a stationary state at an energy below the dissociation threshold, the energy would remain indefinitely in the modes in which it was placed. However, in a classical system, in the absence of using good action-angle variables (which are usually unavailable), anharmonicity transfers energy among the modes. Thus, one possible difficulty with the present QC calculations is that the energy initialized in ν_1 or ν_3 can dissipate to other modes in an unphysical way before dissociation occurs. It is hard to test this at the dissociation energy because at such an energy intermode coupling also occurs in the quantum mechanical world. Therefore, to gain as much insight as possible into how severe this problem is, we made tests at an energy just below the dissociation threshold. In addition to coupled-surface calculations (i.e., photodissociation calculations) we have thus performed single-surface simulations to follow the time evolution of vibrational quantum numbers for ammonia molecules trapped in their $\tilde{A}$ excited electronic state. These simulations were performed for 1000 fs each. This is sufficiently long because the photodissociation dynamics of vibrationally excited ammonia lasts only about 250–300 fs for FSTU/SD simulations, or 350–400 fs for FSTU/SD

+mTRAPZ simulations when the symmetric or antisymmetric stretches are excited with a single quantum. The mTRAPZ method was not used for the mode-coupling simulations described in this subsection.

The harmonic ZPE in the $\tilde{A}$ state is about 0.5 eV above the electronic energy barrier for adiabatic dissociation. To prepare states that are classically bound, the total energy of the $n_1=1$ and $n_3=1$ states were scaled by a factor C, where $C=10^{-4}$, 0.01, 0.1, or 1/6. As the system evolves in time on a single surface, we can analyze for the time-dependent potential energy $V_{\mathrm{vib},m}$ and kinetic energy T_m of each mode m at time $t \geq 0$; these are given by

$$V_{\mathrm{vib},m} = \frac{1}{2}\mu(2\pi c\omega_m)^2 \left[\sum_{\alpha\gamma} \sqrt{\frac{m_\alpha}{\mu}} L_{m,\alpha\gamma}(\tilde{q}_{\alpha\gamma}(t) - \tilde{q}_{e,\alpha\gamma}^0) \right]^2,$$
(14)

where $m=1,2,\ldots,3N-6$ and

$$T_m = \frac{1}{2}\mu \left[\sum_{\alpha\gamma} \sqrt{\frac{m_\alpha}{\mu}} L_{m,\alpha\gamma} v_{\alpha\gamma} \right]^2,$$
(15)

where $v_{\alpha\gamma}$ is an unscaled velocity component. The effective vibrational quantum number of mode m is then

$$n_m = \frac{C(T_m + V_{\mathrm{vib},m})}{hc\omega_m} - \frac{1}{2}.$$
(16)

The meaning of the other symbols and subscripts used in Eqs. (14)–(16) is the same as in Eqs. (4)–(11). For degenerate normal modes (modes 1 and 2, corresponding to the antisymmetric stretch, and modes 4 and 5, corresponding to the in-plane bend) the effective vibrational quantum numbers calculated in Eq. (16) are added to generate the total quantum numbers in each mode k. In the k notation, the time-dependent effective quantum number for $k=1$ is equal to the one for $m=3$, the quantum number for $k=2$ is equal to the one for $m=6$, the quantum number for $k=3$ is equal to the
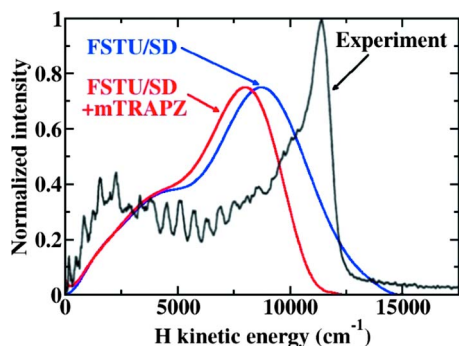
FIG. 3. (Color online) H kinetic energy distributions at the end of FSTU/SD and FSTU/SD+mTRAPZ simulations compared to experimental results of Hause *et al.* (Ref. 14) for $n_1=1$. The maximum of the experimental distribution is normalized to 1, and the maxima of the theoretical distributions to 0.75 for ease of comparison.

sum of the quantum numbers for $m=1$ and $m=2$, and the quantum number for $k=4$ is equal to the sum of the quantum numbers for $m=4$ and $m=5$. *We have adopted the k notation in the rest of the paper*.

III. RESULTS

III.A. Hydrogen-atom kinetic energy distributions

In the experiment by Hause *et al.*,[14] the photodissociation of $NH_3(\tilde{A})$ was found to be mainly electronically adiabatic when singly exciting the antisymmetric stretch ($n_3=1$) and electronically nonadiabatic when singly exciting the symmetric stretch ($n_1=1$). Figure 3 presents the results of FSTU/SD and FSTU/SD+mTRAPZ simulations as well as the experimental spectrum extracted from Ref. 14 for $n_1=1$. The two theoretical models give the same low-energy tail and qualitative shape but the high-energy tail is larger when ZPE is not maintained. This result was expected since departing H atoms may take away more energy when ZPE is not maintained. Moreover, the broad energy range of the theoretical distributions is similar to the experimental one. The FSTU/SD and FSTU/SD+mTRAPZ methods predict the near exclusive formation of the electronic ground state of the amino radical.

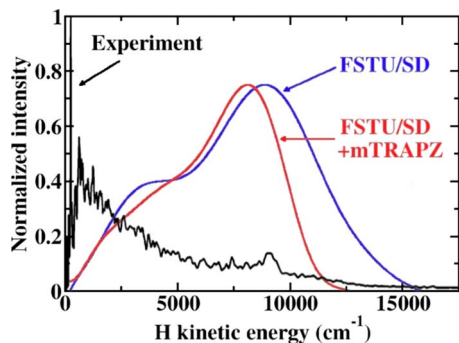Figure 4 presents the experimental spectrum extracted from Ref. 14 as well as the FSTU/SD and FSTU/SD

FIG. 4. (Color online) H kinetic energy distributions at the end of FSTU/SD and FSTU/SD+mTRAPZ simulations compared to experimental results of Hause *et al.* (Ref. 14) for $n_3=1$. The maximum of the experimental distribution is normalized to 1, and the maxima of the theoretical distributions to 0.75 for ease of comparison.

+mTRAPZ distributions obtained for $n_3=1$. Again, the two theoretical methods are in rough agreement with each other and predict a broad range of translational energies. The theoretical models fail to reproduce the experimental spectrum, however, as the predicted photodissociation is again found to be electronically nonadiabatic, that is, to produce the electronic ground state of the amino radical. The rest of this article is primarily devoted to trying to understand this disagreement.

III.B. Choice of coupled-surface trajectory and initial conditions algorithms

Results for the CSDM and FSTU methods, along with the FSTU/SD and FSTU/SD+mTRAPZ results discussed above, are shown in Table I. In these calculations, one or six quanta of excitation are added independently to the symmetric ($n_1=1,6$) or the antisymmetric stretch ($n_3=1,6$). Table I presents results obtained with both schemes for generating initial conditions, that is, the EU scheme and the $\Delta E=0.1$ eV scheme. In this table and following tables, P_2 is the probability of the trajectories finishing on the excited PES. In surface-hopping calculations, this is ordinarily taken as the prediction for the probability of the products being produced in the excited electronic state, and we will follow that convention, supported by the CSDM results in Table I, which show that the probability of excitation in this more accurate method correlates more with P_2, as usually assumed, than with the ensemble-averaged value of the final excited electronic state population, $\langle|c_2|^2\rangle$. However, as an interpretive aid, the table also shows $\langle|c_2|^2\rangle$ for the FSTU simulations. This subsection discusses the results of Table I for the case of one quantum of excitation. The results with multiple quanta of excitation are discussed in Sec. III.C, and the last two columns of the table are also discussed in Sec. III.C.

First consider P_2 for calculations with one quantum of excitation. Table I shows that the FSTU method gives somewhat higher values of P_2 than the FSTU/SD method. The CSDM method predicts slightly more formation of excited-state products, but the probability is still low. Next consider $\langle|c_2|^2\rangle$, again for calculations with one quantum of excitation. These values are also reported in Table I. The values of $\langle|c_2|^2\rangle$ for the initial states with one quantum of excitations in the stretches for FSTU are 25%–26%, which is significantly larger than P_2. This inconsistency may arise for a variety of reasons, and it indicates a general failure of the FSTU method. Under some conditions, $\langle|c_2|^2\rangle$ may be regarded as a rough estimate of an upper limit on P_2. Despite this breakdown of the semiclassical methods, for the (1 0 0 0) and (0 0 1 0) states there is no evidence of the experimental trend since the values of $\langle|c_2|^2\rangle$ upon excitation of the symmetric and antisymmetric stretches are still similar.

III.C. Effect of large initial excitations

The self-consistency breakdown discussed above may be due to the fact that the total energies of interest are near the energetic threshold for dissociation in the excited state. Although the relevant experiments are for one quantum of vibrational excitation in the symmetric stretch or one quantum

TABLE I. Excited-state populations as a function of initial vibrational state. For each method, results are ordered by increasing total energy.

Method	Initial conditions[a]	n_1	n_2	n_3	E_{tot} (eV)	EU		$\Delta E = 0.1$ eV			
						$\langle |c_2|^2 \rangle$	P_2	$\langle |c_2|^2 \rangle$	P_2	P_2^{dir}	P_2^{indir}
FSTU/SD	WS	1	0	0	7.04	⋯	1.4	⋯	0.5	0.1	0.4
	WS	0	0	1	7.07	⋯	0.9	⋯	0.7	0.2	0.5
	WS	6	0	0	8.76	⋯	12.7	⋯	6.9	2.2	4.7
	WS	0	0	6	8.95	⋯	12.7	⋯	19.3	17.6	1.7
FSTU/SD+mTRAPZ	WS	1	0	0	7.04	⋯	0.6	⋯	0.0	0.0	0.0
	WS	0	0	1	7.07	⋯	0.3	⋯	0.0	0.0	0.0
	WS	6	0	0	8.76	⋯	11.7	⋯	4.9	1.1	3.8
	WS	0	0	6	8.95	⋯	11.2	⋯	10.7	7.8	2.9
FSTU	QCU	1	0	0	7.04	28	0.6	25	0.5	0.0	0.5
	QCU	0	0	1	7.07	29	1.0	26	0.5	0.0	0.5
	QCU	6	0	0	8.76	40	16.9	35	6.6	0.6	6.0
	QCU	0	0	6	8.95	42	17.0	40	14.4	9.2	5.2
CSDM	QCU	1	0	0	7.04	⋯	2.5	⋯	1.6	⋯	⋯
	QCU	0	0	1	7.07	⋯	2.7	⋯	1.4	⋯	⋯

[a]This column indicates whether the initial conditions for the modes with $n_k = 0$ were generated according to a QC or a Wigner (W) distribution and whether the umbrella mode frequency is taken as scaled or unscaled when computing initial conditions; WS denotes using Wigner distributions for modes with only zero point energy and a scaled value of 892 cm^{-1} for the umbrella frequency, and QCU denotes using quasiclassical distributions for modes with only zero point energy and an unscaled value of 892 cm^{-1} for the umbrella frequency.

of excitation in the antisymmetric stretch, we examined not only these levels of excitation but also higher levels in order to better understand the difference between exciting the symmetric and antisymmetric stretches. In particular, we performed calculations with a variety of initial conditions corresponding to more than one quantum of excitation. In the first set of additional calculations, we set 3 or 6 quanta (rather than one) in ν_1 or ν_3, or we set up to 16 quanta in the umbrella mode ν_2. In the second set, we consider some of the combinations obtained by exciting the symmetric or antisymmetric stretch by 1, 2, 4, or 6 quanta, and the umbrella mode by 3, 6, or 12 quanta. The first set of calculations is an average over 3000 trajectories for each vibrational state, whereas 1000 trajectories were run for each of the states in the second set. The results are summarized in Table II for the FSTU method and some of the $\Delta E = 0.1$ eV results are plotted in Fig. 5. In addition we present a limited set of results for the FSTU/SD and FSTU/SD+mTRAPZ method in Table I.

Consider first the results in Table I with six quanta in the symmetric or the antisymmetric stretch. One can see that for the $\Delta E = 0.1$ eV scheme, the results show a consistent enhancement in the production of excited amino product (adiabatic dissociation) for the (0 0 6 0) state as compared with the (6 0 0 0) state. For the EU procedure, no such enhancement is observed. For a photodissociation problem such as NH$_3$($\tilde{A}$) → NH$_2$ + H, it seems more appropriate to generate the initial conditions with the $\Delta E = 0.1$ eV procedure, as the energy of the lasers is fixed in the experiments. Therefore, in the following we will emphasize these results and only present the EU results for comparison. The antisymmetric-stretch enhancement for the states with six quanta in the stretches can be generalized by studying the initial states presented in Table II. These results show that for the calcu-

lations with no more than one quantum in the stretches, the excited-state populations correlate with the total energy, and no significant state specificity is observed. However, for the calculations with two or more quanta in the stretches, a significant enhancement in excited-state products is observed when exciting the antisymmetric stretch as compared to exciting the symmetric stretch. In those cases, the state with the antisymmetric stretch excited has between a factor of 1.4 [i.e., compare the (2 1 0 0) and (0 1 2 0) states] and a factor of 2.3 [i.e., compare the (4 3 0 0) and (0 3 4 0) states] larger P_2 than that with the symmetric stretch excited.

We have also studied the effect of generating the initial conditions for unexcited modes either with a QC sampling or a Wigner (W) sampling, for the (1 6 0 0) and (0 6 1 0) vibrational states. The results are shown in Table II. For both states, we observe that the production of electronically excited amino radical using the W sampling is larger if the $\Delta E = 0.1$ eV scheme is employed, and it is smaller if the EU scheme is employed. The quantitative differences between the QC and the W sampling are moderate, about 15% with the EU scheme and about 35% with the $\Delta E = 0.1$ eV scheme, and they should not affect the conclusions drawn on the photodissociation dynamics of NH$_3$($\tilde{A}$).

The last two columns of Tables I and II break P_2 down into direct and indirect contributions. Direct contributions are defined as trajectories that dissociate into electronically excited amino radical without ever quenching to the ground electronic state, and indirect trajectories are those that de-excite at least once, but that eventually re-excite and finalize in the excited state. This analysis shows that the direct and indirect contributions to electronically adiabatic dissociation are similar in magnitude. However when P_2 is high, it is dominated by direct processes. This signals a change in the

TABLE II. Excited-state populations obtained with the FSTU method as a function of initial vibrational state. Results are ordered by increasing total energy.

Initial conditions[a]	n_1	n_2	n_3	E_{tot} (eV)	EU $\langle |c_2|^2 \rangle$	EU P_2	ΔE=0.1 eV $\langle |c_2|^2 \rangle$	ΔE=0.1 eV P_2	ΔE=0.1 eV P_2^{dir}	ΔE=0.1 eV P_2^{indir}
QCU	0	0	0	6.70	28	0.0	28	0.1	0.0	0.1
QCU	1	0	0	7.04	28	0.6	25	0.6	0.1	0.5
QCU	0	0	1	7.07	29	1.0	26	0.7	0.2	0.5
QCU	0	6	0	7.42	35	3.9	36	4.1	0.6	3.5
QCS	2	1	0	7.50	36	4.4	33	2.8	0.3	2.5
QCS	0	1	2	7.56	37	5.4	36	4.5	1.5	3.0
WSU	1	6	0	7.71	40	6.8	40	9.8	3.4	6.4
QCS	1	6	0	7.71	39	7.7	40	7.3	2.3	5.0
QCU	3	0	0	7.73	32	5.9	29	2.3	0.3	2.0
WSU	0	6	1	7.74	43	6.9	42	10.6	4.7	5.9
QCS	0	6	1	7.74	41	8.6	40	7.9	2.7	5.2
QCU	0	0	3	7.83	34	5.6	32	4.4	1.7	2.7
QCU	0	11	0	8.03	39	11.0	44	19.5	10.0	9.5
WSU	1	12	0	8.37	43	15.5	38	21	10.8	9.9
WSU	0	12	1	8.40	42	14.0	43	22	10.6	11.4
WSU	4	3	0	8.44	40	12.5	44	10.6	4.2	6.4
WSU	0	3	4	8.54	45	18.0	48	24	17.2	6.8
QCU	0	16	0	8.64	42	18.7	44	23	9.9	13.1
QCU	6	0	0	8.76	40	16.9	35	6.6	1.2	5.4
QCU	0	0	6	8.96	42	17.0	40	14.4	9.2	5.2
WSU	6	12	0	10.09	45	27	47	31	18.9	12.1
WSU	0	12	6	10.29	55	41	62	51	40	10.6

[a]This column indicates whether the initial conditions for the modes with n_k=0 were generated according to a QC or a Wigner (W) distribution and whether the umbrella mode frequency is taken as scaled or unscaled when computing initial conditions; QCU denotes using quasiclassical distributions for modes with only zero point energy and an unscaled value of 892 cm^{-1} for the umbrella frequency, QCS denotes using quasiclassical distributions for modes with only zero point energy and a scaled value of 892 cm^{-1} for the umbrella frequency, and WSU denotes using Wigner distributions for modes with only zero point energy and a scaled value of 892 cm^{-1} for the umbrella frequency.

reaction mechanism when large excitations are considered. Although these initial states and total energies are far above those considered in the experiments, it is of interest to consider the origin of this selectivity and the change in the reaction mechanism with respect to the other quantized initial states. We will discuss this in detail in Sec. III.F.
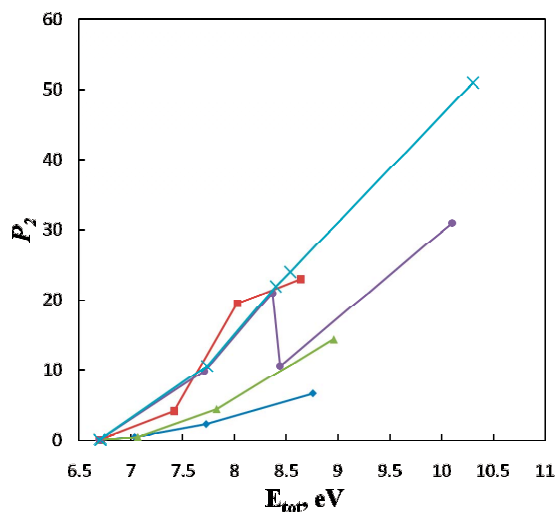

FIG. 5. (Color online) Probability of producing excited-state products as a function of total energy for n_1=n_3=n_4=0 and n_2=0,6,11,16 (squares); n_2=n_3=n_4=0 and n_1=0,1,3,6 (rhombi); n_1=n_2=n_4=0 and n_3=0,1,3,6 (triangles); n_3=n_4=0 and n_1=0, n_2=0; n_1=1, n_2=6; n_1=4, n_2=3; n_1=1, n_2=12; and n_1=6, n_2=12 (circles); n_1=n_4=0 and n_2=0, n_3=0; n_2=6, n_3=1; n_2=12, n_3=1; n_2=3, n_3=4; and n_2=12, n_3=6 (crosses).

III.D. Effect of the diabatic coupling

Since none of the coupled-surface trajectory methods predicts a high population of excited amino radicals for the excited states used in the experiments, one can wonder whether this might be due to a systematic error in the PESs and their couplings. To study the effect of the coupling on our dynamical results we have compared FSTU/SD+mTRAPZ simulations to simulations, where U_{12} is divided or multiplied by 5. The percentages of trajectories that dissociate after H hops (i.e., after one hop, after two hops, etc.) are reported in Table III. Table IV presents information about the average time $\langle t_\downarrow \rangle$ of the first hop (which is necessarily a downward hop), the percentage $P_\downarrow$ of trajectories that dissociate nonadiabatically without attempting any upward hop, and the average fraction F of attempted upward hops that are allowed. We note that the average time $\langle t_\downarrow \rangle$ at the first downward hop is of the order of 15–20 fs, which is much smaller than the average final time of the dynamics, which is ~370 fs for FSTU/SD+mTRAPZ simulations with the original U_{12}.

Table III first reveals that increasing the diabatic coupling increases the propensity of the trajectories to perform several hops before dissociation. However the dissociation process remains completely nonadiabatic; no trajectory has an even number of hops when n_1=1 or n_3=1 if we maintain ZPE. For instance, when using the original U_{12}, and n_3=1, 89.8% of trajectories only hop once, 7.0% three times, and 3.2% more than three times, but always an odd number

TABLE III. Percentage of trajectories that dissociate after H hops for $n_1=1$, $n_3=1$, and for different values of the diabatic coupling. [All calculations in this table employ a Wigner distribution for the modes with $n_k=0$. The umbrella mode frequency (ν_2) is 892 cm^{-1}; $\Delta E=0.1$ eV.]

| | FSTU/SD+mTRAPZ | | | | | | FSTU+mTRAPZ | |
| | $U_{12}/5$ | | U_{12} | | $5U_{12}$ | | U_{12} | |
H	$n_1=1$	$n_3=1$	$n_1=1$	$n_3=1$	$n_1=1$	$n_3=1$	$n_1=1$	$n_3=1$
1	98.1	97.7	90.2	89.8	80.2	80.4	88.8	89.1
3	1.2	1.5	6.9	7.0	14.8	14.8	7.8	7.3
5	0.2	0.3	2.2	2.0	3.3	3.3	2.2	2.5
0,2,4,6	0.0	0.0	0.0	0.0	0.0	0.0	0.0	0.0
≥ 7	0.4	0.5	0.7	1.2	1.6	1.5	1.2	1.1

of times. In this case, the average time $\langle t_\downarrow \rangle$ to the first downward hop is 18 fs, then the average time between the first downward hop and the first upward hop is $\langle t_{\downarrow\uparrow} \rangle=214$ fs, whereas the average time between the first upward hop and the second downward hop is only $\langle t_{\uparrow\downarrow} \rangle=13$ fs. This large difference between $\langle t_{\downarrow\uparrow} \rangle$ and $\langle t_{\uparrow\downarrow} \rangle$ is partly due to the fact that, in this case, the algorithm typically rejects 2.7 upward frustrated hops before accepting one upward hop, whereas downward hops cannot be frustrated. Nevertheless, a pattern emerges, namely, that although upward hops are infrequent, they do occur, but they are almost always followed closely in time by a downward hop.

Interestingly, when we maintain ZPE, if n_1 or n_3 equals 1, then all trajectories hop down at least once. Thus the only way to dissociate adiabatically would be to hop back up and stay up. Table IV provides more information about upward hops. In particular, we see that the percentage of FSTU/SD+mTRAPZ trajectories with $n_3=1$ that dissociate nonadiabatically without even attempting one upward hop is 71%, which clearly demonstrates that no algorithm for accepting upward hop attempts can yield more than 29% of adiabatic dissociation under these conditions. This is in contrast to experimental results that show that most of the ammonia molecules dissociate adiabatically when $n_3=1$. When the diabatic coupling is increased, upward hops become more frequent, and only 10% of trajectories that dissociate nonadiabatically never experience any upward hop. However, the fraction F of the allowed upward hops to the number of attempted upward hops also decreases when the cou-

pling increases, as shown in the third row of Table IV. More upward hops are thus attempted, but most of them are frustrated, and the dissociation remains nonadiabatic.

Statistics were also calculated for the last downward hop, in particular, the average time $\langle t_{last} \rangle$, the average adiabatic energy gap $\langle \Delta V \rangle$, the average maximum N–H distance $\langle R_{max} \rangle$, and the average nonplanarity angle $\langle \alpha_{np} \rangle$. Note that the last downward hop is often the first hop since a number of trajectories hop only once. The statistics for the last downward hop are collected in Table V. The nonplanarity angle is defined in degrees as

$$\alpha_{np} = 360 - \sum_{i=1}^{3} \theta_i, \tag{17}$$

where θ_i are the three H–N–H angles. Note that for planar NH$_3$ the sum of the three angles is 360°. Table V shows that most of the key aspects of the dynamics upon excitation of ν_1 are similar to those upon excitation of ν_3. For U_{12} unscaled we find $\langle t_{last} \rangle=51$ fs and $\langle \Delta V \rangle=0.34$ eV in both cases, and $\langle R_{max} \rangle=2.1$ Å, which is close to the conical intersection that is located at an N–H distance of about 2 Å in C_{2v} geometry.

When the diabatic coupling is decreased most of the last downward hops still occur close to the conical intersection but the average energy gap and the nonplanarity angle are much smaller; one expects then that the probability of nonadiabatic dissociation to the ground electronic state should be increased. In contrast, increasing the diabatic coupling in-

TABLE IV. Average time $\langle t_\downarrow \rangle$ of the first downward hop, percentage $P_\downarrow$ of trajectories that dissociate on the ground electronic state without attempting any upward hop, average fraction F of attempted upward hops that are allowed, and average final $\langle |c_2|^2 \rangle$ probability for the excited electronic state, when $n_1=1$ or $n_3=1$ for different values of the diabatic coupling. [All calculations in this table employ a Wigner distribution for the modes with $n_k=0$. The umbrella mode frequency (ν_2) is 892 cm^{-1}; $\Delta E=0.1$ eV.]

| | FSTU/SD+mTRAPZ | | | | | | FSTU+mTRAPZ | |
| | $U_{12}/5$ | | U_{12} | | $5U_{12}$ | | U_{12} | |
	$n_1=1$	$n_3=1$	$n_1=1$	$n_3=1$	$n_1=1$	$n_3=1$	$n_1=1$	$n_3=1$
$\langle t_\downarrow \rangle$ (fs)	14	14	19	18	24	21	19	18
$P_\downarrow$ (%)	97.4	96.7	70.7	71.2	9.7	9.9	62.8	62.4
F	0.40	0.38	0.15	0.16	0.04	0.04	0.006	0.008
$\langle |c_2|^2 \rangle$	⋯	⋯	⋯	⋯	⋯	⋯	0.28	0.27

TABLE V. Average time $\langle t_{\text{last}} \rangle$, average adiabatic energy gap $\langle \Delta V \rangle$, average maximum N–H distance $\langle R_{\text{max}} \rangle$, and average nonplanarity angle $\langle \alpha_{\text{np}} \rangle$ at the last downward hop. [All calculations in this table employ a Wigner distribution for the modes with $n_k = 0$. The umbrella mode frequency (ν_2) is 892 cm^{-1}; $\Delta E = 0.1$ eV.]

| | FSTU/SD+mTRAPZ | | | | | | FSTU+mTRAPZ | |
| | $U_{12}/5$ | | U_{12} | | $5U_{12}$ | | U_{12} | |
	$n_1 = 1$	$n_3 = 1$	$n_1 = 1$	$n_3 = 1$	$n_1 = 1$	$n_3 = 1$	$n_1 = 1$	$n_3 = 1$
$\langle t_{\text{last}} \rangle$ (fs)	22	23	51	51	669	604	68	66
$\langle \Delta V \rangle$ (eV)	0.12	0.14	0.34	0.34	0.62	0.62	0.34	0.34
$\langle R_{\text{max}} \rangle$ (Å)	2.00	1.99	2.10	2.11	2.09	2.09	2.11	2.11
$\langle \alpha_{\text{np}} \rangle$ (deg)	2.3	2.5	7.5	9.0	11.7	12.0	2.4	2.2

creases the nonplanarity angle and the average energy gap; the adiabatic dissociation pathway should therefore be more favored. These trends are in agreement with information in Table IV where a smaller diabatic coupling corresponds to a higher percentage $P_\downarrow$ of trajectories that dissociate nonadiabatically without attempting any hop back up, whereas a larger diabatic coupling corresponds to a much smaller percentage $P_\downarrow$. However, as previously pointed out, although the adiabatic pathway is more likely to be used for part of the trajectory when U_{12} increases, no molecule dissociates adiabatically in FSTU/SD+mTRAPZ calculations with $n_1 = 1$ and $n_3 = 1$. Also, note that $\langle t_{\text{last}} \rangle$ increases significantly when the diabatic coupling is increased; this might be related to the increase in the number of allowed hops (see Table III).

III.E. Intermode couplings

One possible reason for the discrepancy between the mixed quantum/classical simulations and the experimental findings is the possibility of strong classical intermode couplings. Therefore, as mentioned in Sec. II.D, we wanted to check whether energy placed in ν_1 or ν_3 is actually available for mode-specific dissociation or whether it dissipates before dissociation due to the fact that the vibrational mode energies are not conserved in a classical anharmonic system.

The symmetric and antisymmetric stretches are indeed close in energy ($\nu_1 = 2777$ cm^{-1} and $\nu_3 = 3041$ cm^{-1}) and classical modes close in energy may be more strongly coupled to each other during the dynamics than quantum modes would be. Then energy placed in ν_3 could dissipate to other modes before the hopping region is reached. To clarify this issue we performed the single-surface test runs described in Sec. II.D. If the energy stayed in the modes where it was initially placed (as it would in quantum mechanics because these test runs are below the dissociation threshold or as it would even in classical mechanics if the system were harmonic because we only consider systems with no initial rotational energy in this article), then the effective quantum
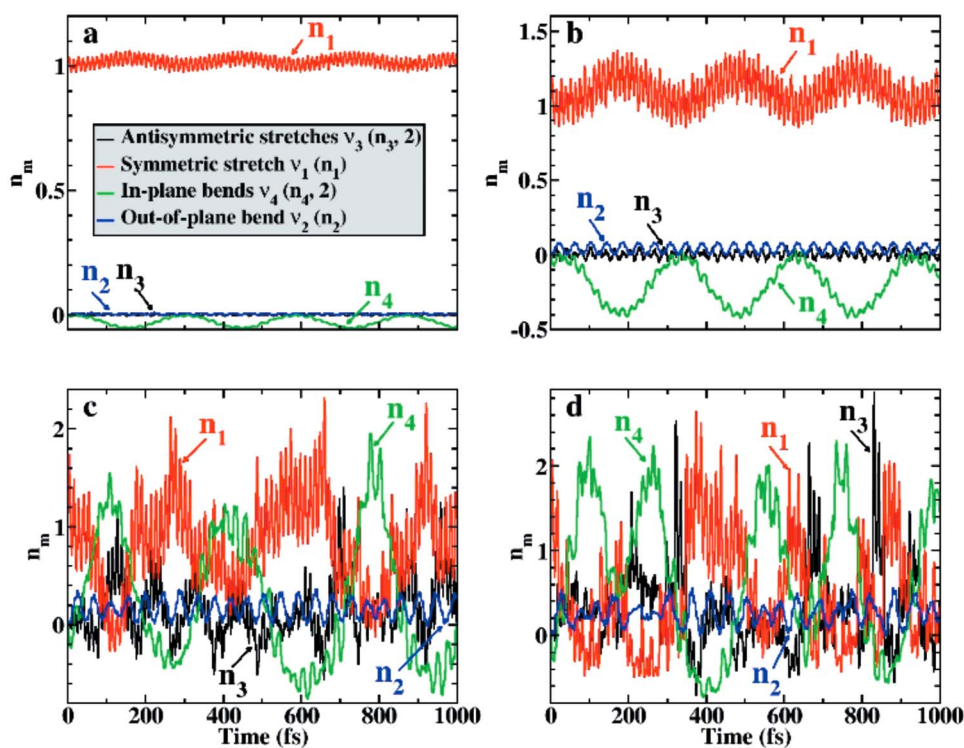

FIG. 6. (Color online) Effective quantum number n_k from single-surface calculations with $n_1 = 1$, $n_2 = n_3 = n_4 = 0$, and $C =$ (a) 10^{-4}, (b) 0.01, (c) 0.1, and (d) 1/6.
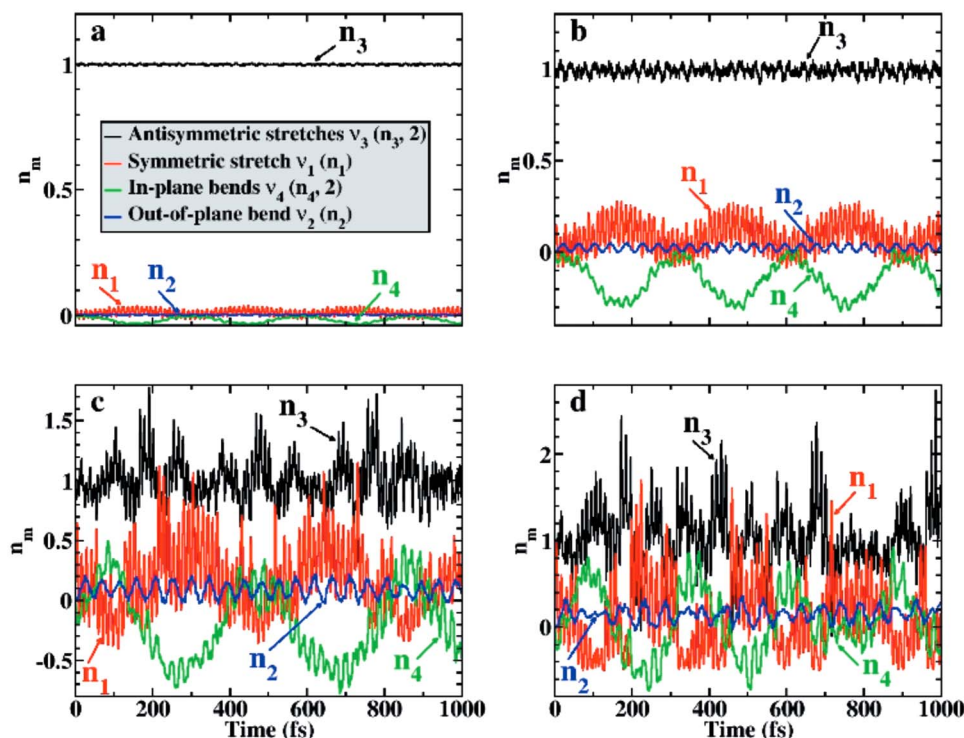
FIG. 7. (Color online) Effective quantum number n_k from single-surface calculations with $n_3=1$, $n_1=n_2=n_4=0$, and $C=$ (a) 10^{-4}, (b) 0.01, (c) 0.1, and (d) 1/6.

numbers defined in Eq. (16) would be constant. Figures 6 and 7 present these effective quantum numbers for single-surface simulations in which the symmetric and antisymmetric stretches are excited with one quantum of vibration respectively, and when the initial vibrational energies are scaled by C as described in Sec. II.D. (In these figures, as in all of Sec. III, we use the spectroscopic quantum numbers n_k with $k=1-4$, rather than the normal mode quantum numbers n_m with $m=1-6$. Thus, when a mode is doubly degenerate we have plotted the sum of the contributions of each degenerate mode. We therefore obtain four curves for each value of C instead of six.)

Figure 6 shows that on average, the effective quantum numbers of the out-of-plane bend (umbrella mode) and of the antisymmetric stretches are maintained close to zero throughout the dynamics whereas some energy seems to flow from the symmetric mode to the in-plane bends. For these two modes, not only the average effective quantum number is somewhat different from the initial value but also the magnitude of oscillations is large (≈ 1). The same behavior is shown in Fig. 7 where the antisymmetric stretch is excited. Although the intermode coupling is stronger when $C=1$ (not shown because dissociation would occur), the findings that (i) n_3 oscillates around approximately the same value for the entire length of a 1000 fs simulation and (ii) there is little dissipation of ν_3 energy into ν_1 or vice versa show that intermode couplings are not strong enough to eliminate the possibility of simulating state-specific behavior on the time scale of the photodissociation process. We therefore continue to search for the reason why theory disagrees with experiment for $n_3=1$.

III.F. Reaction mechanism

The $3N-7$ generalized normal mode vibrational frequencies derived from the projected Hessian along the electronically adiabatic MEP for dissociation in the $\tilde{A}$ state were computed using the POLYRATE (Ref. 63) program package, as explained in Sec. II.C, and the results are shown in Fig. 8. This figure shows the adiabatic correlations with changing characters of the normal mode vibrations along the reaction coordinate. The correlations between the normal modes are clearer if we compute $3N-6$ frequencies from the un-
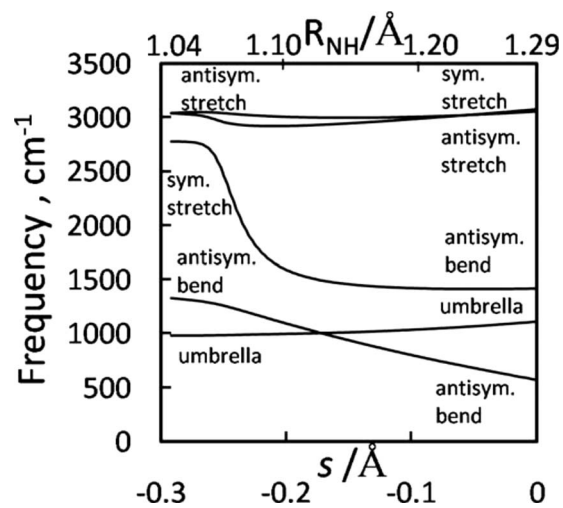

FIG. 8. Generalized-normal-mode vibrational frequencies in the adiabatic electronically excited state along the reaction path connecting the NH$_3$ well ($s=-0.3$ Å) to the saddle point ($s=0$). The frequencies were computed with the reaction coordinate (taken as the MEP in isoinertial coordinates downhill from the saddle point to the excited-state minimum) projected out. The curves reflect an adiabatic correlation of the vibrational modes.
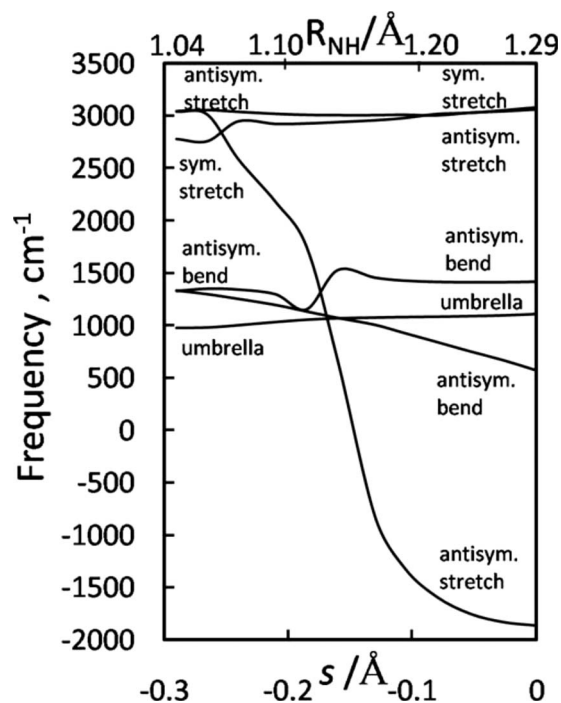
FIG. 9. Vibrational frequencies in the adiabatic electronically excited state along the reaction path connecting the NH$_3$ well ($s=-0.3$ Å) to the saddle point ($s=0$). These frequencies were computed without projecting out the reaction coordinate; when a frequency becomes imaginary it is plotted as a negative number. The curves reflect an approximate diabatic correlation of the vibrational modes.

projected Hessian along the reaction path, even if this procedure is only strictly valid at stationary points. The mode frequencies calculated this way are presented in Fig. 9. In this figure, the modes have been correlated diabatically, that is, by their character (i.e., symmetric stretch, antisymmetric bend, etc.). At the NH$_3$($\widetilde{A}$) well ($s=-0.3$ Å), the four unique frequencies correspond to a doubly degenerate antisymmetric stretch, a symmetric stretch, a doubly degenerate antisymmetric (in-plane) bend, and a symmetric (out-of-plane) umbrella motion. As the system proceeds to the saddle point, the degeneracy of the antisymmetric stretch is broken; one antisymmetric stretch becomes the reaction coordinate (its frequency drops and moves out the imaginary axis, represented by negative numbers in Fig. 9), and the other is largely conserved. The frequency associated with the symmetric stretch is also largely conserved, although the avoided crossing between the symmetric and antisymmetric stretches at $s=-0.25$ Å suggests these motions may be coupled as the system leaves the well. The antisymmetric stretch is also coupled with an antisymmetric bend at around $s=-0.2$ Å. The second antisymmetric bend and the umbrella motion are uncoupled from the other vibrations.

Although the vibrational state energies in Figs. 8 and 9 are for the adiabatic electronically excited state, very similar results would be obtained for the diabatic electronically excited state because the adiabatic and diabatic representations are very similar for the regions of coordinate space shown in these figures.

Figures 8 and 9 suggest differences in the dissociation dynamics when exciting the symmetric or antisymmetric stretches. Excitation of the symmetric stretch does not release vibrational energy into reaction coordinate motion for proceeding over the saddle point in the $\widetilde{A}$ state, whereas excitation of the antisymmetric stretch puts half the energy associated with the antisymmetric vibration into the reaction coordinate. As discussed above, we find no significant trends with respect to excitation of the symmetric and antisymmetric stretches in our multistate trajectory simulations at low energies. However, we find some selectivity with respect to exciting several quanta of antisymmetric stretch (i.e., at higher energies). Interestingly, the selectivity seems to increase with total energy for this type of vibrational state. There are several possibilities that could explain this behavior. First, the coupling between the symmetric and antisymmetric stretches near $s=-0.25$ Å might provide enough mixing to destroy the state-specific mechanism proposed above at low energies. In contrast, for higher vibrational excitation, the trajectories should be more vibrationally diabatic, thus conserving the character of the modes to a larger extent as they overcome the saddle point and reach the region of the conical intersection. Second, the classical trajectory simulations may not preserve the quantized motions as the system dissociates, although the results of Sec. III.E suggest that these motions are largely quantized over the time scales of interest here. This nonconservation should have a larger effect the smaller the number of quanta put into the stretches, as it is well known that the shape of the probability distribution of the vibrational coordinate computed from vibrational wave functions tends to resemble that computed from classical vibrations at large vibrational excitation.[64]

To further explore the effect of the quantized vibrations along the $\widetilde{A}$ state MEP, we initiated trajectories at the saddle point using QC initial conditions, as discussed in Sec. II.B. We assume vibrationally diabatic motion, where trajectories with symmetric-stretch excitation are given n_1 quanta in the 3078 cm^{-1} frequency motion at the saddle point, which has the character of a symmetric stretch. For ν_2, the 1108 cm^{-1} frequency motion at the saddle point was excited with n_2 quanta. For the antisymmetric stretch, the results of the following two sets of runs were averaged: (a) n_3 quanta were added to the 3057 cm^{-1} frequency motion at the saddle point, and (b) no excitations were made in the bound modes at the saddle point, and the excess energy defined by Eq. (13) was added along the reaction coordinate. We consider some of the initial states presented in Table II. The results are summarized in Table VI.

For the vibrational states in Table VI, the probabilities for forming excited-state products are not very sensitive to whether the trajectories are initiated at the saddle point or the NH$_3$($\widetilde{A}$) well, and no state specificity is observed in either case. This finding is in agreement to the general tendency observed for the calculations initiated in the minimum of the $\widetilde{A}$ electronic state when the EU scheme of generating initial conditions is used, as already noted for the states in Table II. The mechanism implied above suggests that antisymmetric-stretch excitation using schemes (a) and (b) leads to different dynamics, but we find that schemes (a) and (b) lead to similar excited-state populations. When the EU scheme is used,

TABLE VI. Excited-state FSTU populations as a function of initial vibrational state for trajectories initiated at the $\widetilde{A}$ state saddle point. Results are ordered by increasing total energy. [All calculations in this table employ a QC distribution for the modes with $n_k = 0$. The umbrella mode frequency (ν_2) is 978 cm^{-1}, and the initial conditions are EU (i.e., ΔE is unrestricted).]

n_1	n_2	n_3	E_{tot} (eV)	P_2
0	0	0	6.71	0.1
0	0	1	7.08	0.3
1	0	0	7.09	0.5
0	6	0	7.54	5.0
0	0	3	7.84	4.0
3	0	0	7.85	4.4
0	11	0	8.22	14.0
0	16	0	8.91	19.5
0	0	6	8.98	13.7
6	0	0	8.99	16.5

the probability for forming excited-state products is dependent on the total energy and is not dependent on the details of the preparation of the excited-state complex, irrespective of the region where the trajectories are initiated. One possible explanation of the energy-dependent increase in the production of excited amino for low vibrational excitations (for both the EU and $\Delta E = 0.1$ eV schemes) could be offered by noting that for these conditions, as discussed in more detail in Sec. III.D, nearly every trajectory seems to pass near to a conical intersection after passing the saddle point. Especially at lower total energies, once the system is quenched by the conical intersection, an $NH_3(\widetilde{X})$ complex is often formed, and this complex can be fairly long lived. For this type of trajectories, it would be likely that the details of the initial state are lost as the system spends time as $NH_3(\widetilde{X})$. Eventually $NH_3(\widetilde{X})$ dissociates, and while it dissociates there is some probability that the system will attempt a transition to the excited electronic state. Because the energy of the excited-state products are close to the total energies considered here, the probability of successfully transitioning to the excited state would depend sensitively on total energy.

The reaction mechanism changes significantly when higher initial vibrational excitations are considered. Under those conditions, there are many trajectories that dissociate in the excited state with no hops between the potential surfaces. The most interesting new aspect found at these higher total energies, when the $\Delta E = 0.1$ eV scheme is used to generate the initial conditions, is selectivity for antisymmetric-stretch excitations with respect to symmetric-stretch excitations. As shown in Tables I and II, initial states with two or more quanta in one of the stretching modes lead to an increased production of excited amino radicals when the antisymmetric stretch is excited. The enhancement factor varies between a factor of 1.4 for the (0 1 2 0) versus the (2 1 0 0) state and a factor of 2.3 for the (0 3 4 0) versus the (4 3 0 0) state [very close to the 2.2 factor found for the (0 0 6 0) versus the (6 0 0 0) state]. Comparing (0 3 4 0) versus (4 3 0 0) and (0 0 6 0) versus (6 0 0 0), which have comparable total energies, one can see that the effect of the umbrella excitation is to increase the total yield of excited amino radicals, but that the selectivity with respect to the

antisymmetric-stretch excitation remains essentially constant. Interestingly, essentially all of the observed increase in excited-state yield is associated with trajectories that do not hop at all, as evidenced by a comparison of P_2^{dir} and P_2^{indir} in Table II for the pairs of states (2 1 0 0)-(0 1 2 0), (3 0 0 0)-(0 0 3 0), (4 3 0 0)-(0 3 4 0), (6 0 0 0)-(0 0 6 0), and (6 12 0 0)-(0 12 6 0). Indeed, for the case of the (6 0 0 0) and (0 0 6 0) states, there are almost eight times more trajectories of the direct type in the (0 0 6 0) case than in the (6 0 0 0) case. The total energies of these initial states are 8.96 and 8.76 eV, respectively. As observed in Table II, for the state with the antisymmetric stretch excited, 14% of trajectories dissociate in the excited state, compared to 7% for the state with the symmetric stretch excited.

To take a better look at the reaction mechanism, we have performed an analysis of the turning points in the motion of the dissociating hydrogen atom during the trajectories. The trajectories that have no outer turning points of this motion are classified as noncomplex (they dissociate without a "rebound" at longer N–H bond distances), and the rest are classified as complex. All trajectories are classified by the potential surface (ground or excited) to which they dissociate, and complex trajectories are further classified by the number of outer turning points. Trajectories that experience outer turning points only when in the ground state are said to form GS complexes; those that experience outer turning points only when in the excited state are said to form ES complexes; and those that experience outer turning points on both surfaces are said to form MS complexes. We have chosen three representative pairs of initial vibrational states that have excited stretches: the pair of states (0 0 1 0)-(1 0 0 0) with only stretch excitation, and the pairs (0 1 2 0)-(2 1 0 0) and (0 3 4 0)-(4 3 0 0) that have simultaneous excitation in the stretches and in the umbrella mode. The results are presented in Table VII. Taking for instance the (1 0 0 0) initial state as representative for low-energy initial states, around 20% of trajectories proceed through formation of a $NH_3(\widetilde{X})$ complex, with lifetimes ranging between 200 fs and more than 1 ps, and then dissociate in the ground electronic state. Most of the remaining trajectories dissociate directly on the ground state after hopping at the conical intersection with lifetimes of 150–200 fs, with only a few dissociating in the excited state. If we analyze specifically the adiabatic trajectories, we see that more than half of them are complex, which is a significantly larger fraction than for the global average. This illustrates the role of complex trajectories in producing excited amino radicals for trajectories initiated in low-energy vibrational states.

Focusing now on the differences between the results for initial vibrational states with the antisymmetric stretch versus symmetric stretch excited, Table VII reveals important differences in the percentage of trajectories of each type. A large percentage of trajectories dissociating in the ground state are noncomplex, but their number is always larger for excited antisymmetric stretch and it decreases by a large factor when the vibrational excitation increases. Trajectories that are complex are mostly short lived (i.e., they have a relatively small number of outer turning points), and their number is always smaller for excited antisymmetric stretch.

TABLE VII. Classification of trajectories by their number of outer turning points and the potential surface to which they dissociate, for three pairs of initial vibrational states. [The (0010), (1000) calculations in this table are FSTU/SD calculations that employ a Wigner distribution for the modes with $n_k=0$. The (0120) and (2100) calculations employ FSTU and a QC distribution. The (0340) and (4300) calculations employ FSTU and a Wigner distribution. The umbrella mode frequency (ν_2) is always 892 cm^{-1}, and the initial conditions correspond to $\Delta E=0.1$ eV.]

Type of trajectory[a]	N_{otp}	(0010)	(1000)	(0120)	(2100)	(0340)	(4300)
		Trajectories that dissociate to the ground state					
Noncomplex	0	64.6	58.9	39.7	32.0	25.5	21.7
GS complexes	1–20	19.2	22.0	36.1	41.0	27.6	40.4
	20–40	1.8	1.6	1.9	2.1	0.2	0.5
	40–60	1.0	1.0	0.4	0.6	0.02	0.0
	60–80	0.7	0.6	0.1	0.2	0.0	0.0
	>80	0.5	0.6	0.06	0.0	0.0	0.0
ES complexes	1–2	2.1	2.8	1.2	1.9	3.4	3.1
	2–4	0.02	0.06	0.0	0.02	0.2	0.2
	>4	0.02	0.02	0.0	0.0	0.08	0.03
MS complexes	1–20	4.2	5.3	7.2	8.7	16.3	19.3
	20–40	1.8	2.4	5.0	5.6	2.5	3.0
	40–60	1.1	1.5	2.3	2.5	0.3	0.5
	60–80	0.6	0.8	0.7	0.7	0.0	0.1
	>80	0.8	1.2	0.4	0.6	0.04	0.0
		Trajectories that dissociate to the excited state					
Noncomplex	0	0.2	0.08	1.8	0.6	17.5	4.1
GS complexes	1–10	0.2	0.1	1.2	1.3	2.5	2.7
	10–20	0.02	0.0	0.08	0.1	0.1	0.2
	>20	0.0	0.04	0.1	0.08	0.0	0.05
ES complexes	1–2	0.06	0.06	0.2	0.1	0.8	0.8
	2–4	0.0	0.02	0.2	0.04	0.2	0.3
	>4	0.02	0.02	0.02	0.04	0.1	0.1
MS complexes	1–20	0.1	0.2	0.5	0.3	2.0	2.2
	20–40	0.04	0.02	0.2	0.1	0.2	0.3
	>40	0.06	0.04	0.2	0.1	0.0	0.03

[a]"GS" stands for ground state, "ES" stands for excited state, and "MS" stands for mixed state (i.e., those trajectories that have outer turning points both in the ground and in the excited state).

The tendency of the antisymmetric stretch to produce noncomplex trajectories is much more marked for the trajectories that dissociate in the excited state. Thus, the (0 3 4 0) state originates about four times more noncomplex trajectories in the excited state than the (4 3 0 0) state. Note that the number of noncomplex trajectories in the excited state is approximately equal to the number of direct trajectories, as one can check comparing the number of noncomplex trajectories in Table VII with the number of direct trajectories in Table II. This means that if a complex (even a short-lived one) is formed in the excited state, trajectories will most likely hop down and dissociate in the ground state. This is borne out by comparing the numbers of excited-state complex trajectories that ultimately dissociate in the ground state with those that dissociate in the excited state.

We have also analyzed the trajectories for the (6 0 0 0) and (0 0 6 0) initial vibrational states by taking the average of several quantities relevant to the dynamics. First, we have defined a region in configuration space where trajectories are most likely to experience a downward hop as that where about 2/3 of the downward hops occur, with about 1/6 at smaller N–H distances and 1/6 at larger N–H distances; we found that this region is characterized by N–H distances be-

tween about 1.9 and 2.2 Å. Then, for each trajectory, the nonplanarity angle is computed for the configuration within this region that has the minimum adiabatic energy gap. We also compute the instantaneous relative translational energy of the departing H atom (relative to the center of mass of the amino group) at this configuration. The nonplanarity angle and relative translational energy are also computed at the first downward hop of each trajectory. For the state with six quanta of excitation in the symmetric stretch [i.e., the (6 0 0 0) state], for direct adiabatic trajectories the average minimum energy gap is about 0.9 eV, the average nonplanarity angle at the minimum-gap geometries is about 3°, and the average instantaneous relative translational energy of the departing H atom at this configuration is about 1.5 eV. These values may be compared to their analogs at the first downward hop for indirect trajectories, which are about 0.3 eV, typically less than 1° (with much more dispersion than for the direct trajectories), and 1.5 eV, respectively. The results for six quanta of excitation in the antisymmetric stretch [i.e., the (0 0 6 0) state] are comparable for indirect trajectories but they are quite different for direct trajectories. For direct trajectories, the values of the average minimum energy gap, nonplanarity angle, and average H relative translational en-

ergy are about 0.7 eV, about 3°, and about 2.0 eV, respectively. For indirect trajectories, at the first downward hop these values are about 0.3 eV, typically less than 1° (again with much more dispersion than for the direct trajectories), and 1.5 eV, respectively.

A comparison of the data obtained from the trajectories reveals that the minimum energy gaps are much larger for direct than for indirect trajectories, as expected, and also that direct trajectories manage to avoid hopping even though they have small nonplanarity angles of only 3°. The main difference between the dynamics of the (6 0 0 0) and (0 0 6 0) states is the much larger number of direct (and noncomplex) trajectories for the second state, which has the antisymmetric stretch excited. For this state, direct trajectories have an average relative kinetic energy of the departing H atom about 0.5 eV larger than at the downward hops for the indirect trajectories. For the state with the symmetric stretch excited, there is no significant difference between direct and indirect trajectories regarding this quantity. Therefore, we conclude that the reason for the enhanced production of excited amino radicals when the antisymmetric stretch is excited with several quanta is the high speed of the dissociating hydrogen atom as it crosses the region of conical intersection due to the release of energy along the reaction coordinate that does not take place when the symmetric stretch is excited, as revealed by the vibrational energy level curves as a function of the reaction coordinate.

IV. CONCLUDING REMARKS

We have performed a mixed quantum-classical study of the photodissociation dynamics of $NH_3(\tilde{A})$ vibrationally excited in its symmetric and antisymmetric stretching modes. According to recent experiments, the symmetric stretch, the umbrella mode, and the two bends mainly lead to electronically nonadiabatic dissociation whereas the antisymmetric stretch mainly leads to electronically adiabatic dissociation. We find a mechanism for the antisymmetric stretch to promote electronically adiabatic photodissociation, namely, that in contrast to the symmetric stretch, the antisymmetric stretch correlates with a lower frequency at the saddle point and releasing energy into the reaction coordinate speeds up the system enough to fly past the funnel centered on the conical intersection fast enough for dissociation to occur in the electronically excited state. However, despite the use of an improved mean-field approach (the CSDM method) and three improved surface-hopping methods (the FSTU +mTRAPZ, FSTU/SD, and FSTU/SD+mTRAPZ methods), some of which maintain ZPE throughout the dynamics, the full dynamical calculations only succeed in qualitatively reproducing the experimental results for $n_1=1$. The experimental mode specificity of the two types of stretches is not found in our simulations that employ the experimental quantized states and energies. We find selectivity only after significantly increasing the level of excitation in the stretch modes. Increasing or decreasing the diabatic coupling U_{12} does not improve the agreement with experiment. The effect of intermode couplings has also been investigated on single-surface simulations in the excited electronic state at energies below the dissociation threshold, and—to the extent that these tests are indicative of the higher-energy dynamics—this study indicates that these couplings may play a minor role in our difference from experiment.

It is disappointing that the present calculations do not reproduce the experimental mode specificity at the experimental energies. Further work is required to determine the origin of the discrepancy.

[1] J. Biesner, L. Schneider, J. Schmeer, G. Ahlers, X. X. Xie, K. H. Welge, M. N. R. Ashfold, and R. N. Dixon, J. Chem. Phys. **88**, 3607 (1988).
[2] J. Biesner, L. Schnieder, G. Ahlers, X. Xie, K. H. Welge, M. N. R. Ashfold, and R. N. Dixon, J. Chem. Phys. **91**, 2901 (1989).
[3] A. Nakajima, K. Fuke, K. Tsukamoto, Y. Yoshida, and K. Kaya, J. Phys. Chem. **95**, 571 (1991).
[4] R. N. Dixon, Acc. Chem. Res. **24**, 16 (1991).
[5] E. L. Woodbridge, M. N. R. Ashfold, and S. R. Leone, J. Chem. Phys. **94**, 4195 (1991).
[6] S. A. Henck, M. A. Mason, W. B. Yan, K. K. Lehmann, and S. L. Coy, J. Chem. Phys. **102**, 4783 (1995).
[7] D. Edvardsson, P. Baltzer, L. Karlsson, B. Wannberg, D. M. P. Holland, D. A. Shaw, and E. E. Rennie, J. Phys. B **32**, 2583 (1999).
[8] R. A. Loomis, J. P. Reid, and S. R. Leone, J. Chem. Phys. **112**, 658 (2000).
[9] A. Bach, J. M. Hutchison, R. J. Holiday, and F. F. Crim, J. Chem. Phys. **116**, 4955 (2002).
[10] A. Bach, J. M. Hutchison, R. J. Holiday, and F. F. Crim, J. Chem. Phys. **116**, 9315 (2002).
[11] A. Bach, J. M. Hutchison, R. J. Holiday, and F. F. Crim, J. Chem. Phys. **118**, 7144 (2003).
[12] H. Akagi, K. Yokoyama, and A. Yokoyama, J. Chem. Phys. **118**, 3600 (2003).
[13] A. Bach, J. M. Hutchison, R. J. Holiday, and F. F. Crim, J. Phys. Chem. A **107**, 10490 (2003).
[14] M. L. Hause, Y. H. Yoon, and F. F. Crim, J. Chem. Phys. **125**, 174309 (2006).
[15] D. J. Kouri and D. G. Truhlar, J. Chem. Phys. **91**, 6919 (1989).
[16] H. Guo and G. C. Schatz, J. Chem. Phys. **93**, 393 (1990).
[17] M. Karplus, R. N. Porter, and R. D. Sharma, J. Chem. Phys. **43**, 3259 (1965).
[18] D. G. Truhlar and J. T. Muckerman, in *Atom-Molecule Collision Theory: A Guide for the Experimentalist*, edited by R. B. Bernstein (Plenum, New York, 1979), pp. 505–566.
[19] J. C. Tully, in *Modern Methods for Multidimensional Dynamics Computations in Chemistry*, edited by D. L. Thompson (World Scientific, Singapore, 1998), pp. 34–72.
[20] D. G. Truhlar, in *Quantum Dynamics of Complex Molecular Systems*, edited by D. A. Micha and I. Burghardt (Springer, Berlin, 2007), pp. 227–243.
[21] C. Zhu, S. Nangia, A. W. Jasper, and D. G. Truhlar, J. Chem. Phys. **121**, 7658 (2004).
[22] A. W. Jasper, C. Zhu, S. Nangia, and D. G. Truhlar, Faraday Discuss. **127**, 1 (2004).
[23] C. Zhu, A. W. Jasper, and D. G. Truhlar, J. Chem. Theory Comput. **1**, 527 (2005).
[24] A. W. Jasper, S. Nangia, C. Zhu, and D. G. Truhlar, Acc. Chem. Res. **39**, 101 (2006).
[25] A. W. Jasper, S. N. Stechmann, and D. G. Truhlar, J. Chem. Phys. **116**, 5424 (2002).
[26] A. W. Jasper, S. N. Stechmann, and D. G. Truhlar, J. Chem. Phys. **117**,

10427 (2002) (Erratum).

[27] A. W. Jasper and D. G. Truhlar, Chem. Phys. Lett. **369**, 60 (2003).

[28] A. W. Jasper and D. G. Truhlar, J. Chem. Phys. **127**, 194306 (2007).

[29] H. D. Meyer and W. H. Miller, J. Chem. Phys. **70**, 3214 (1979).

[30] D. A. Micha, J. Chem. Phys. **78**, 7138 (1983).

[31] A. Bjerre and E. E. Nikitin, Chem. Phys. Lett. **1**, 179 (1967).

[32] J. C. Tully and R. K. Preston, J. Chem. Phys. **55**, 562 (1971).

[33] N. C. Blais and D. G. Truhlar, J. Chem. Phys. **79**, 1334 (1983).

[34] J. C. Tully, J. Chem. Phys. **93**, 1061 (1990).

[35] D. Bonhommeau and D. G. Truhlar, J. Chem. Phys. **129**, 014302 (2008).

[36] T. Seideman, J. Chem. Phys. **103**, 10556 (1995).

[37] W. Lai, S. Y. Lin, D. Xie, and H. Guo, J. Chem. Phys. **129**, 154311 (2008).

[38] F. F. Crim, Annu. Rev. Phys. Chem. **44**, 397 (1993).

[39] G. Herzberg, *Molecular Spectra and Molecular Structure. III. Electronic Spectra and Electronic Structure of Polyatomic Molecules* (Van Nostrand Reinhold, New York, 1966), pp. 463–515.

[40] F. F. Crim, J. Phys. Chem. **100**, 12725 (1996).

[41] A. W. Jasper and D. G. Truhlar, J. Chem. Phys. **123**, 064103 (2005).

[42] D. C. Chatfield, R. S. Friedman, D. G. Truhlar, and D. W. Schwenke, Faraday Discuss. Chem. Soc. **91**, 289 (1991).

[43] J. C. Gray, D. G. Truhlar, L. Clemens, J. W. Duff, F. M. Chapman, Jr., G. O. Morrell, and E. F. Hayes, J. Chem. Phys. **69**, 240 (1978).

[44] J. M. Bowman, B. Gazdy, and Q. Sun, J. Chem. Phys. **91**, 2859 (1989).

[45] W. H. Miller, W. L. Hase, and C. L. Darling, J. Chem. Phys. **91**, 2863 (1989).

[46] R. Alimi, A. Garcia-Vela, and R. B. Gerber, J. Chem. Phys. **96**, 2034 (1992).

[47] K. F. Lim and D. A. McCormack, J. Chem. Phys. **102**, 1705 (1995).

[48] Y. Guo, D. L. Thompson, and T. D. Sewell, J. Chem. Phys. **104**, 576 (1996).

[49] D. A. McCormack and K. F. Lim, J. Chem. Phys. **106**, 572 (1997).

[50] G. Stock and M. Thoss, Phys. Rev. Lett. **78**, 578 (1997).

[51] D. A. McCormack and K. F. Lim, Phys. Chem. Chem. Phys. **1**, 1 (1999).

[52] G. Stock and U. Muller, J. Chem. Phys. **111**, 65 (1999).

[53] Z. Xie and J. M. Bowman, J. Phys. Chem. A **110**, 5446 (2006).

[54] Z. H. Li, A. W. Jasper, D. Bonhommeau, R. Valero, and D. G. Truhlar, ANT Adiabatic and Nonadiabatic Trajectories 08: A code to study photochemical and thermochemical reactions, University of Minnesota, Minneapolis, 2008.

[55] Z. H. Li, R. Valero, and D. G. Truhlar, Theor. Chem. Acc. **118**, 9 (2007).

[56] R. Schinke, *Photodissociation Dynamics* (Cambridge University Press, Cambridge, UK, 1993).

[57] D. G. Truhlar, A. D. Isaacson, R. T. Skodje, and B. C. Garrett, J. Phys. Chem. **86**, 2252 (1982).

[58] D. G. Truhlar, A. D. Isaacson, and B. C. Garrett, in *Theory of Chemical Reaction Dynamics*, edited by M. Baer (CRC, Boca Raton, 1985), pp. 65–137.

[59] D. G. Truhlar and B. C. Garrett, Faraday Discuss. Chem. Soc. **84**, 464 (1987).

[60] J. C. Tully, in *Dynamics of Molecular Collisions, Part B*, edited by W. H. Miller (Plenum, New York, 1976), p. 217.

[61] S. Nangia and D. G. Truhlar, J. Chem. Phys. **124**, 124309 (2006).

[62] Y. L. Volobuev, M. D. Hack, and D. G. Truhlar, J. Phys. Chem. A **103**, 6225 (1999).

[63] J. C. Corchado, Y.-Y. Chuang, P. L. Fast, W.-P. Hu, Y.-P. Liu, G. C. Lynch, K. A. Nguyen, C. F. Jackels, A. Fernandez Ramos, B. A. Ellingson, B. J. Lynch, V. S. Melissas, J. Villà, I. Rossi, E. L. Coitiño, J. Pu, T. V. Albu, R. Steckler, B. C. Garrett, A. D. Isaacson, and D. G. Truhlar, POLYRATE, version 9.4, University of Minnesota, Minneapolis, 2005.

[64] L. Pauling and E. B. Wilson, *Introduction to Quantum Mechanics, with Applications to Chemistry* (McGraw-Hill, New York, 1935).